Large-scale cortical networks are organized in structured cycles

*Mats W.J. van Es[a], *Cameron Higgins[a,b], Chetan Gohil[a], Andrew J. Quinn[a,c], Diego Vidaurre[a,d], Mark W. Woolrich[a]
*Contributed equally

[a] Oxford Centre for Human Brain Activity (OHBA), Wellcome Centre for Integrative Neuroimaging, Department of Psychiatry, University of Oxford, Oxford, OX3 7JX, United Kingdom
[b] Resonait Medical Technologies Pty Ltd
[c] Centre for Human Brain Health, School of Psychology, University of Birmingham, UK
[d] Department of Clinical Medicine, Aarhus University, Denmark

Abstract
The human brain exhibits recurrent oscillatory activity in cortical networks of neuronal populations, which are thought to play a role in specialized cognitive functions. However, it is not known whether these oscillatory network states evolve over time in a structured or random matter. In this study, we introduce a new method for analyzing the long-term evolution of these states, and demonstrate that they follow a cyclical architecture when the brain is at rest, with typical cycle durations of 300-500 milliseconds. This cyclical organization structure positions the default mode network (DMN) and dorsal attention network (DAN) at opposite phases of the cycle, with the DMN preceded by higher frequency oscillations in sensorimotor networks and followed by lower frequency oscillations in frontotemporal networks respectively. The cyclical structure was robust in three large magnetoencephalography (MEG) resting state datasets, and persists in a visuo-motor task, where cycle phase predicts reaction time. Moreover, individual cyclical dynamics were predictive of demographics: older people deviate less from the cycle structure and show a general slowing of cycle rate, and cycle rate is strongly heritable. These findings suggest that the evolution of oscillatory network states in the human brain may be more organized than previously thought and provide potential biomarkers for health and disease.

Keywords: MEG, HMM, resting state, functional brain networks, cycle, Cam-CAN, HCP, MEG UK, Wakeman-Henson, heritability, age

Introduction
Natural cognition arises from the flexible interaction of multiple brain networks, each of which subserve distinct modes of information processing. Understanding and characterizing the temporal precedence in which these networks activate tells us about the underlying order of information processing in the brain, and how the brain accommodates diverse functional requirements over multiple timescales.

Cyclical patterns are ubiquitous in physiology and offer a dynamic mechanism for regulating the balance between competing functional needs. Neurophysiological recordings obtained

during sleep distinguish successive cycles in which characteristic oscillatory patterns evolve through well identified stages (Jouvet, 1967). In contrast, wakeful brain activity similarly distinguishes different oscillatory network patterns, however these are far more transient and flexibly combine over much shorter timescales (Baker et al., 2014). It nonetheless remains possible that an overarching, endogenous architecture governs the activation of these networks.

Multimodal evidence suggests that recurrent activation and deactivation of the DMN is one of the defining features of resting brain network activity (de Pasquale et al., 2010; Fox et al., 2005; Vidaurre et al., 2018a). The DMN was originally understood to reflect an offline or idling state, but in recent times has been identified as serving a number of important functions in the awake state (Andrews-Hanna, 2012; Buckner et al., 2008; Menon, 2023), including awake replay (Higgins et al., 2021). These functions are broadly unified by an internal orientation of attention, where the object of attention is being generated internally by the brain (Spreng et al., 2009; Spreng and Grady, 2010). Conversely, the Dorsal Attention Network (DAN) mediates processes where attention is oriented towards a stimulus in the external environment, and its temporal activation is strongly anticorrelated with the DMN (Baker et al., 2014; de Pasquale et al., 2010; Fox et al., 2005; Smith et al., 2009; Vidaurre et al., 2017).

The characterization of resting state networks in electrophysiology offers a means to investigate these networks at high temporal resolution. In this modality, activation of the DMN is characterized by a distributed pattern of heightened power and coherence across multiple frequency bands (Baker et al., 2014; de Pasquale et al., 2010; Mantini et al., 2007), a mechanism believed to support coordinated information flow across multiple regions (Vidaurre et al., 2018b). It is strongly anticorrelated with a network state characterized by reduced power and coherence in predominantly parietal areas, which has been postulated to represent the DAN (Baker et al., 2014; de Pasquale et al., 2010; Mantini et al., 2007). This view is reinforced by fMRI evidence positioning the DMN and the DAN at opposite extrema of a gradient between brain regions that serve multimodal and unimodal processing, respectively (Margulies et al., 2016).

While previous research has identified the activation patterns of the DMN and the DAN, important questions remain as to how the brain transitions between these cognitive states, and as to whether there is temporal structure that mediates the flow between internally and externally oriented attention? Here, we use magnetoencephalography (MEG) data and a novel analysis method to analyze long-term temporal structure in the activation of cortical networks. Using this method, we show that for each cortical network state, there exists a preferential and unique pathway of state activations before and after its own activation. Together, the preferred pathways to each cortical network state are organized into a cycle of network state activations. We reproduce this effect in three MEG datasets and show that summary metrics of the network cycle are heritable, and relate to age, cognition, and behavioral performance.

Results

To explore the temporal dynamics of large-scale functional brain networks in resting state MEG, we first conducted a secondary analysis of previously published results (Higgins et al., 2021). This new analysis considered the longer-term patterns of resting state network (RSN) activity in the Nottingham MEG UK dataset (55 subjects) (UK MEG Partnership, 2016).

Using hidden Markov modelling (HMM), the analysis (see methods) identified states reflecting distinct brain networks with unique spatial configurations of power and coherence that recur at different points in time. An example network state is shown in Figure 1, which, based on its spatio-spectral characteristics was previously identified as the default mode network (DMN) state (Higgins et al., 2021; Sitnikova et al., 2020). The state descriptions of all network states are shown in Figure S1.

The Default Mode Network has distinct ascending and descending network pathways

We characterized the tendency of network states to follow or precede each other using a novel method called Temporal Interval Network Density Analysis (TINDA; Figure 1). This method focusses on the variable-length intervals between network state occurrences, which relaxes more common assumptions of fixed-length timing patterns, an approach that we show is crucial to its success (see S3). For each network state, TINDA takes all inter-state intervals (ISIs) and partitions them evenly in half. It then defines the Fractional Occupancy (FO) Asymmetry as the difference between the probability of another network state occurring in the first half versus the second half of those intervals. This measure captures if there is a tendency for a network state to follow, or precede, another state over long timescales (Methods and Fig. 1D-E).

We first used this method on the intervals defined by subsequent visits to the DMN state (state 1). This revealed that certain network states tend to occur after the DMN (i.e. in the first half of the DMN interval) while other states tend to occur before the DMN (i.e. in the second half of the DMN interval); Specifically, States 2 ($p=2.3*10^{-5}$) and 8 ($p=9.9*10^{-8}$) are more likely to activate before state 1, whereas states 5 ($p=4.1*10^{-6}$) and 9 ($p=3.7*10^{-8}$) are more likely to activate after state 1. All other states (3, 6, 7, 10, 11, and 12) did not exhibit significant asymmetric activation probability after Bonferroni correction for multiple comparisons. We visualized the significant FO asymmetries as a directed graph (Figure 1H) that shows how brain activity might “flow” through state space, i.e., as ascending pathways to the DMN, and descending pathways from the DMN. We note here that the configuration of states in 1H is for consistency of visualization, which will be justified below. In the interest of reproducibility, we repeated the same analysis for the equivalent DMN state in two other large datasets (Cam-CAN (N=612) (Cam-CAN et al., 2014; Taylor et al., 2017) and HCP (N=79) (Larson-Prior et al., 2013), and found consistent results (see Fig. S2).

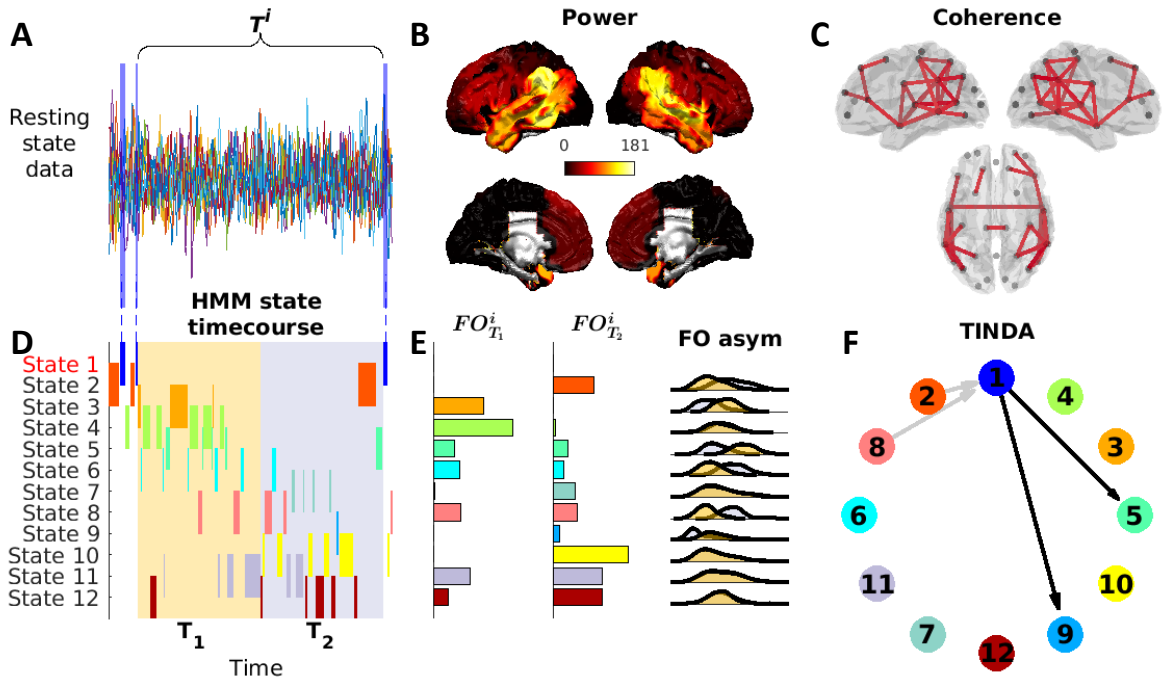

Figure 1. Temporal Interval Network Density Analysis (TINDA) for the default mode network (DMN) state (state 1). A) A time segment of the resting state MEG data for one example subject. The blue annotations are periods where state 1 is active. The segment annotated T_i is the interval under consideration in D. B) The wideband PSD of this DMN state is highest in parieto-temporal parcels. The color bar denotes wideband power increase from the mean over states. C) The coherence of the DMN state is strongest between parieto-temporal and parieto-frontal parcels (top 5% connections larger than state-mean are shown). D) The state time courses for an example interval $\boldsymbol{T^i}$ between two visits to the DMN state corresponding the data in A. TINDA splits the DMN interval into half, i.e., $\boldsymbol{T_1^i}$ and $\boldsymbol{T_2^i}$. E) TINDA then computes separately for each state the Fractional Occupancies (FO) for $\boldsymbol{T_1^i}$ and $\boldsymbol{T_2^i}$ to get $\boldsymbol{FO_{T_1^i}}$ and $\boldsymbol{FO_{T_2^i}}$ (right). This is then repeated over all DMN intervals (over all subjects) to build up distributions of $\boldsymbol{FO_{T_1}}$ and $\boldsymbol{FO_{T_2}}$. Differences between these two distributions indicates an FO asymmetry. F) The direction of any significant asymmetry indicates those states that activate in the second interval half before, or the first half interval after, the DMN state. Note that each arrow corresponds to a significant (Bonferroni corrected) FO asymmetry.

Resting state network activation pathways are unified by an overarching cyclical structure

We next investigated whether asymmetries in activation probabilities also exist for other states. Using TINDA on all pairs of states, we confirmed that this was indeed the case, and moreover, that these pathways were unique to each state (Fig. S2 and Fig 2B/E/H).

We then explored the possibility that the asymmetries in network activation probabilities are unified by an overarching structure. In particular, overlaying these pathways onto existing network maps (Higgins 2021) raised the possibility of an overarching cyclical pattern governing these state dynamics. To clearly visualize this, we again plot the significant, pairwise FO Asymmetries (Fig 2 A/D/G) as connections in a directed graph and established a

quantitative metric summarizing a graph's cycle strength $\boldsymbol{S}$ (see methods) in order to test the potential cyclical structure statistically.
Cycle strength ranges from +1 for graphs with an overall clockwise direction, to -1 for graphs with an overall counterclockwise direction, given a particular order of states (see Methods for details). Figure 2B shows the directed graph according to the ordering of states that maximize $\boldsymbol{S}$; this displays an unmistakable cyclical pattern. We then evaluated whether such cyclical structure could arise by chance, by shuffling the labelling of states for each subject 1000 times and each time arranging the nodes to maximize $\boldsymbol{S}$; the observed cycle strength was significantly greater than in permutations ($p<0.001$; Fig 2C).

These analyses were replicated in the two other datasets in the interest of reproducibility (Cam-CAN: $p<0.001$, Fig 2D-F; HCP: $p<0.001$, Fig 2G-I). Furthermore, despite inherent differences between the different models inferred for each dataset – and in the case of the HCP data the use of an entirely different parcellation – the ordering of states within the cycle was reproduced; after matching the states to the MEG UK state descriptions (see methods), the difference of a state's position within the circle graph compared to the matched state from MEG UK was smaller than what would be expected from chance based on 10000 permutations of state positions (Cam-CAN: $p = 0.0051$; HCP: $p = 0.0002$). These analyses across three MEG datasets thus show that the cyclical activation of cortical networks is robust, and importantly, that the ordering of states within the cycle is preserved.

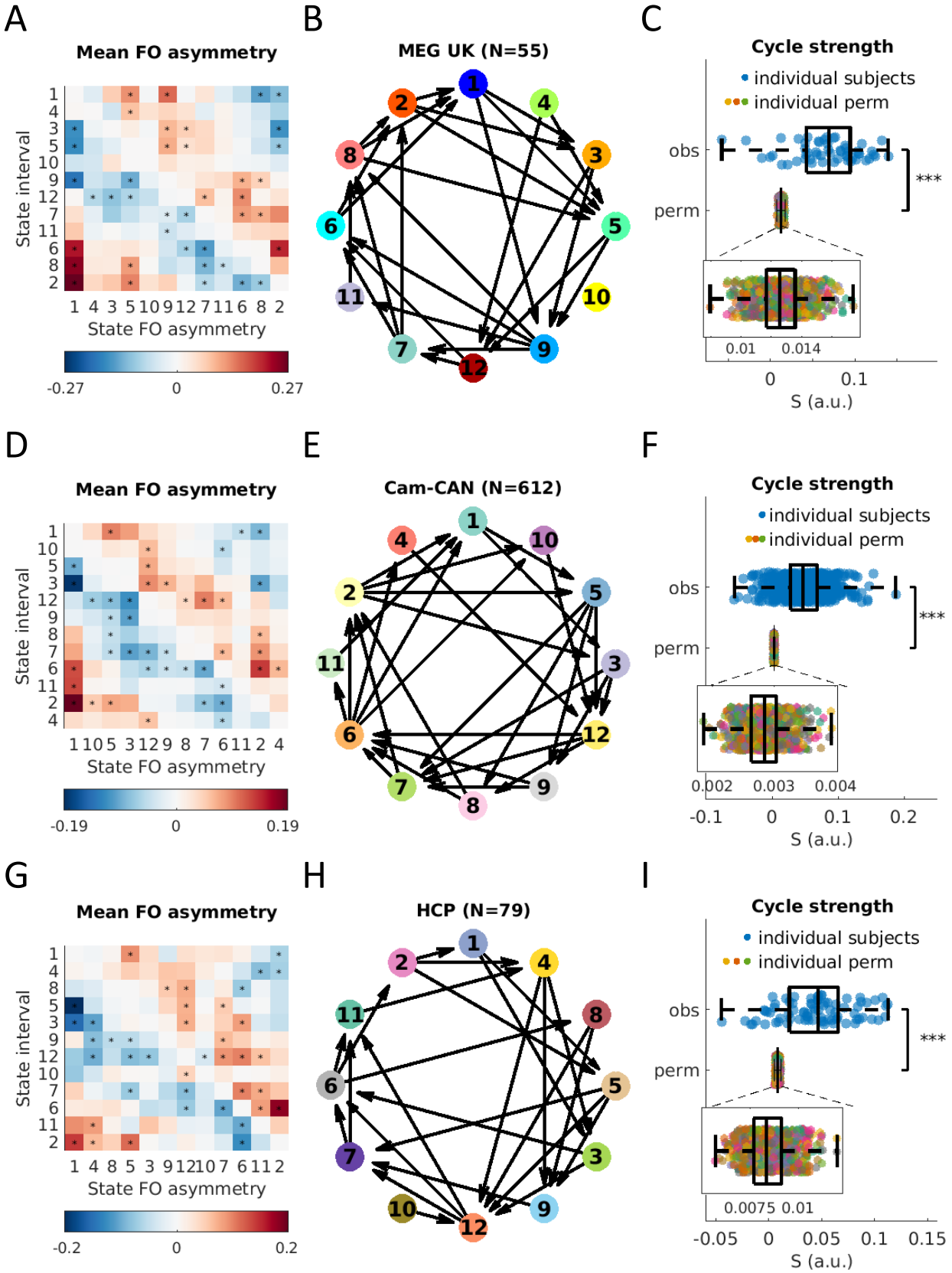
A
Mean FO asymmetry
State interval
State FO asymmetry
-0.27
0
0.27
B
MEG UK (N=55)
C
Cycle strength
individual subjects
individual perm
obs
perm
***
0.01
0.014
0
0.1
S (a.u.)
D
Mean FO asymmetry
State interval
State FO asymmetry
-0.19
0
0.19
E
Cam-CAN (N=612)
F
Cycle strength
individual subjects
individual perm
obs
perm
***
0.002
0.003
0.004
-0.1
0
0.1
0.2
S (a.u.)
G
Mean FO asymmetry
State interval
State FO asymmetry
-0.2
0
0.2
H
HCP (N=79)
I
Cycle strength
individual subjects
individual perm
obs
perm
***
0.0075
0.01
-0.05
0
0.05
0.1
0.15
S (a.u.)

Figure 2. The combination of ascending pathways (i.e., a tendency to move into a state of interest from another specific state) and descending pathways (i.e. a tendency to move from a state of interest to another specific other state) reveals an overarching cyclical activation structure of functional brain networks in three large MEG datasets (A-C MEG UK, D-F: Cam-CAN, G-I: HCP). A, D, G) The group-average Fractional Occupancy (FO) Asymmetry describes the activation probability of one state (x-axis) relative to another (y-axis). B, E, H). States are ordered around the circular graph such that there is a minimum of violations between the ascending and descending pathways and a consistent rotational direction around the circle. C, F, I) The cycle strength in the observed data is stronger than can be expected from chance at the group-level (modelling subjects as random effects and doing permutation testing). Blue circles correspond to individual subjects, colored circles to the group mean for a single permutation. Boxplots display the median, 25th and 75th percentile, and whiskers indicate the minimal and maximal value. Insets shows the variation of the cycle strength for each permutation. *** denotes $p<0.001$.

Cyclical structure is strongest over timescales of seconds

Given the strength of this cyclical activation pattern, we considered why it had not been characterized previously in the literature. TINDA differs from other methods of characterizing dynamics in that it measures dynamics over inter-state intervals of variable length. As shown in figure 3A, these intervals have a highly dispersive distribution with a very long tail. Other common means of modelling temporal dynamics assume either a Markovian structure (i.e. that the state at one timepoint is conditionally dependent on only the immediately prior state, e.g. (Baker et al., 2014) or a fixed length time-lag to models of temporal dependency (Mitra and Raichle, 2016). Simulations from either of these models trained on the existing dataset demonstrated that they capture only a small part of this inherent cyclical structure, most of which is lost due to the variability of inter-state interval durations (Figure S3). The fact that other models capture only a small part of this inherent cyclical structure underlines the significance of our novel approach.

This also suggests two key temporal features of the cyclical patterns we have characterized; firstly, that these cyclical patterns are instantiated over longer time scales; and secondly that they do not have a regular cyclical period (a claim we will substantiate below). To verify the first of these quantitatively, we looked at the dependency of the FO asymmetry and cycle strength on the interval duration (i.e., $\boldsymbol{T}$ in figure 1, the interval time between subsequent visits to the network state of interest). We expected that if cyclical patterns are instantiated over longer timescales, then the FO asymmetries and the characteristic cycle would only be apparent at longer interval times.

To do this we partitioned the distribution of interval times into quintiles and reran TINDA for each quintile. The left column in figure 4 shows that significant asymmetries in the Fractional Occupancy (FO) are much rarer, and the strength of the cyclical structure is close to zero (right column; red) when only considering shorter intervals (right column; blue). It also shows that the strongest cyclical patterns exist when considering interval times on the order of seconds. The same profile was replicated in the Cam-CAN and HCP datasets (Fig S4), and were not artefacts of other common physiological signals (Supplement V). Taken

together, this shows that the asymmetric ordering of RSNs into a cycle is occurring in dynamics at timescales on the order of seconds.

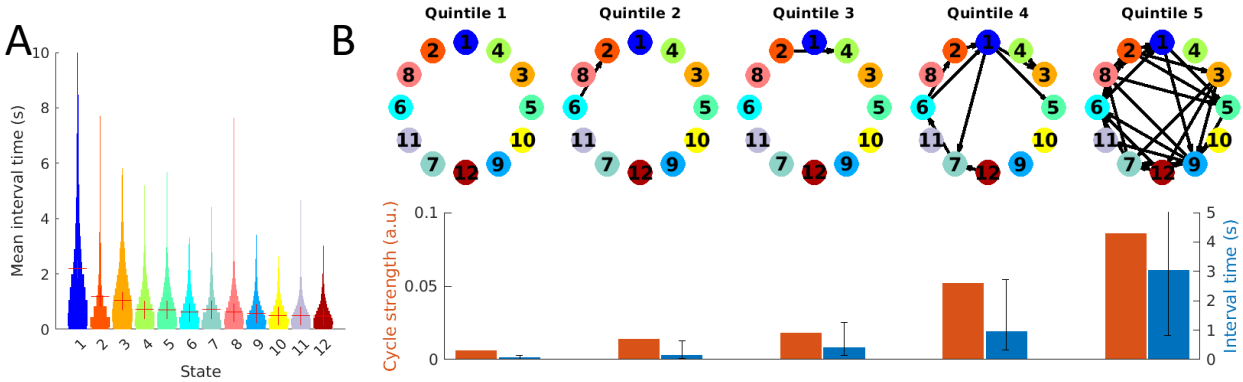

Figure 3. The observed cyclical organization of state activations is driven by longer temporal interval times. A) The distribution of inter-state interval times (i.e., $\boldsymbol{T}$ in figure 1, the interval time between subsequent visits to the network state of interest), emphasizing that these intervals have a long-tailed dispersive distribution. B) Interval times are partitioned into five quintiles. The left column shows the cyclical pattern that appears for each quintile (from low interval times to high interval times (IT)). The right column shows the mean interval time (IT; blue) and cycle strength (red) for each IT quintile, over subjects.

Cyclical structure groups networks with similar spectral properties and function

Having established that resting state networks tend to activate in a cyclical progression, we next characterized what a complete traversal of a single cycle might look like. We did this by simply mapping the spatial/spectral network state descriptions provided by the HMM onto the cycle. The result of this is shown in Figures 5 for the MEG UK dataset with power maps, and S5 for the other datasets and coherence maps. We emphasize that each network state comprises a spatially defined pattern of power and coherence. In order to display these high dimensional representations more succinctly, Figure 5A only shows the single dominant spatio-spectral mode in each state (see Methods and Fig S1); this information is further condensed and summarized in figures 5B-C.

The first major mode of differentiation between states emerges on the North-South direction of the clock face. In the spectral domain, states in the upper quadrant have a higher overall power and inter-area coherence (phase locking), whereas those in the lowest quadrant have lower overall power and inter-area coherence (phase locking). This is not a mere broadband power increase, but rather reflects different combinations of oscillatory activity in distinct or overlapping frequency bands (Vidaurre et al., 2018b).

A second mode of differentiation emerges on the East-West direction of the clock face. In terms of spectral activity, states on the left of the quadrant display activity in higher frequency bands; for instance, state 6 is associated with beta band activity, and state 2 with alpha band activity. On the other hand, states on the right-hand side show activity in lower frequency bands, particularly the delta/theta band.

Spatially, states on the left-hand side show activity in sensorimotor and parietal areas, which are often associated with physical sensation and spatial awareness. Meanwhile, states on the right-hand side show activity mostly in higher-order cognitive areas, such as fronto-temporal and language areas (Sepulcre et al., 2012; Smith et al., 2009; Vidaurre et al., 2018b). These regions are generally associated with complex cognitive functions like reasoning, problem-solving, and language processing (Braun et al., 2015; Colom et al., 2010). This differentiation in spectral activity suggests different types of brain function and processes might be involved in these states. For example, these results suggest that states ascending into state 1, which was characterized by enhanced amplitudes in regions overlapping the DMN (including bilateral inferior parietal lobe, medial prefrontal cortex, and medial temporal lobe) are linked to higher frequency oscillatory activity in sensorimotor areas. In contrast, networks descending from the DMN comprise of slower frequency content in higher order cognitive areas, which in turn ascends into low power states, and in particular state 7, which was characterized by a decrease in oscillatory power in the parietal regions overlapping the dorsal attention network (DAN; including intraparietal sulcus and extending towards the frontal eye fields (FEF)).
In the interest of reproducibility, this plot has been replicated on the Cam-CAN and HCP datasets. The main findings summarized in figure 5B and 5C were reliably reproduced (Figure S6), despite some moderate differences in network state definitions.

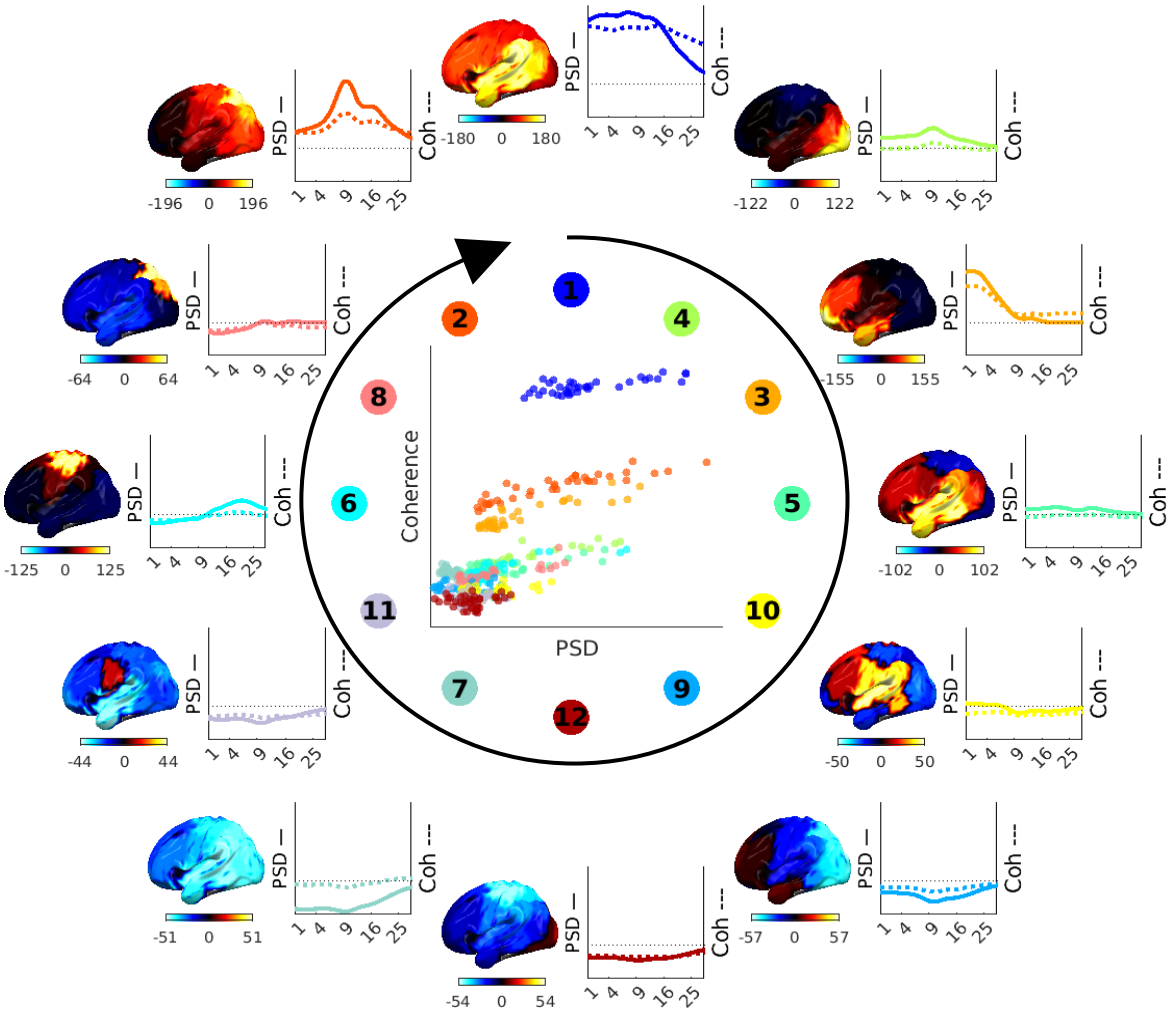

Spectral Characteristics

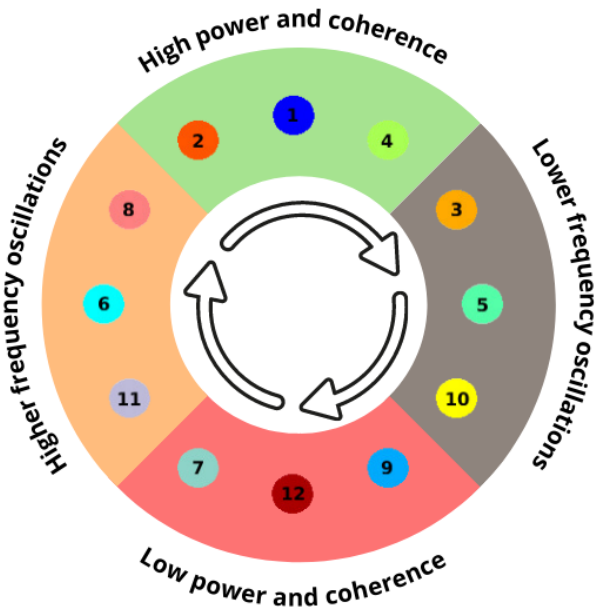

Spatial Characteristics

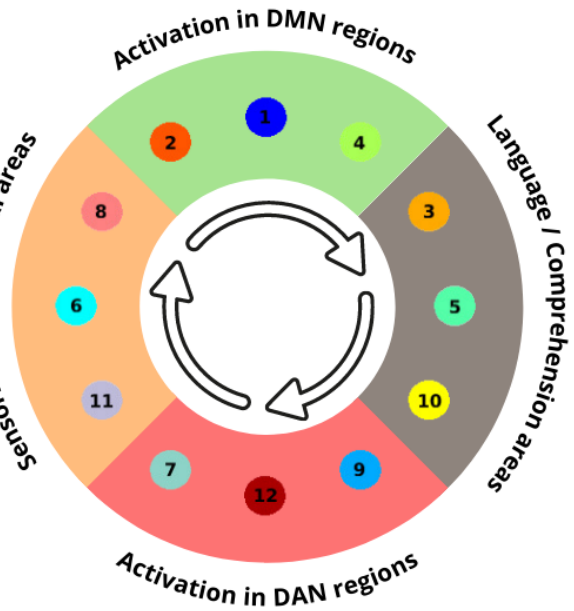

Figure 4. The cyclical structure groups together networks that have similar spectral properties and cognitive versus primary-sensorimotor function. A) The spatio-spectral characteristics of functional brain networks are embedded in their cyclical progression (see main text). Each brain map shows the percentage increase in power relative to the mean over states, projected onto the left hemisphere (see Fig. S6 for the coherence maps and replication in Cam-CAN and HCP, and Fig S1. for detailed spectral characteristics for each state). To the right of each brain map is the spatial average PSD (solid line) and coherence (dotted line) as a function of frequency, relative to the average over states (horizontal dotted red line). The middle plot depicts the wideband group-average PSD versus coherence for each state (color) and parcel (dot). B) Spectrally, the main modes of differentiation along the cycle have high vs. low power and coherence (North/South), and high vs. low frequency content (West/East). C) Spatially, the main modes of differentiation along the cycle have activation in regions associated with an internal vs. external focus (North/South) and sensorimotor/parietal vs. higher order cognitive regions (West/East).

Cycle statistics associate with individual traits and are heritable

We then sought to characterize the temporal statistics of individual cycles, in order to better characterize individual traversals of the cycle and how these differ across the population. Inspired by the qualitative segmentation of the cycle into four "meta states" of distinct spatio-spectral characteristics (Figure 4B-C), we define a full cycle as being made up of a sequential activation of these four meta states. This allows us to define a cycle's duration as the time taken to progress through this sequence of four meta-states, which we infer using another, second level HMM run on the time courses of sliding window fractional occupancy for the underlying network states (see Figure 5A/S7 and Methods for details).

With this approach we sought to characterize what a 'typical' traversal of a cycle entailed in the MEG UK dataset. The group average mean cycle duration was 549msec (Figure 5B), roughly 8.7 times longer than the mean duration of individual network states. Evaluating the states visited on each individual cycle revealed these only comprised 5.4 unique state visits on average (Figure 6B). This tells us a typical cycle traversal visits less than half of the K=12 available states but returns to several of those states at least once.

Plotting the phase shifts of each observed state transition further reinforces the view that cyclical dynamics emerge only from quite stochastic and noisy short term state dynamics. If we consider each state transition on the cyclical clock face as a phase shift in the complex plane, we can histogram these transitions as in Figure 5D. The mode of this plot is a state transition that is one step in the clockwise direction. However, a state transition two steps clockwise is as probable as a transition one step counterclockwise; thus a net clockwise motion is achieved only with frequent steps back in the counterclockwise direction. Furthermore, jumps of four or more steps in either direction – that we would characterize as broadly 'acyclic' transitions – nonetheless account for 25% of all state transitions. Thus, the cyclic dynamics we have identified emerge from noisy short term state transitions that are perhaps better conceptualized as a random walk around the clock face.

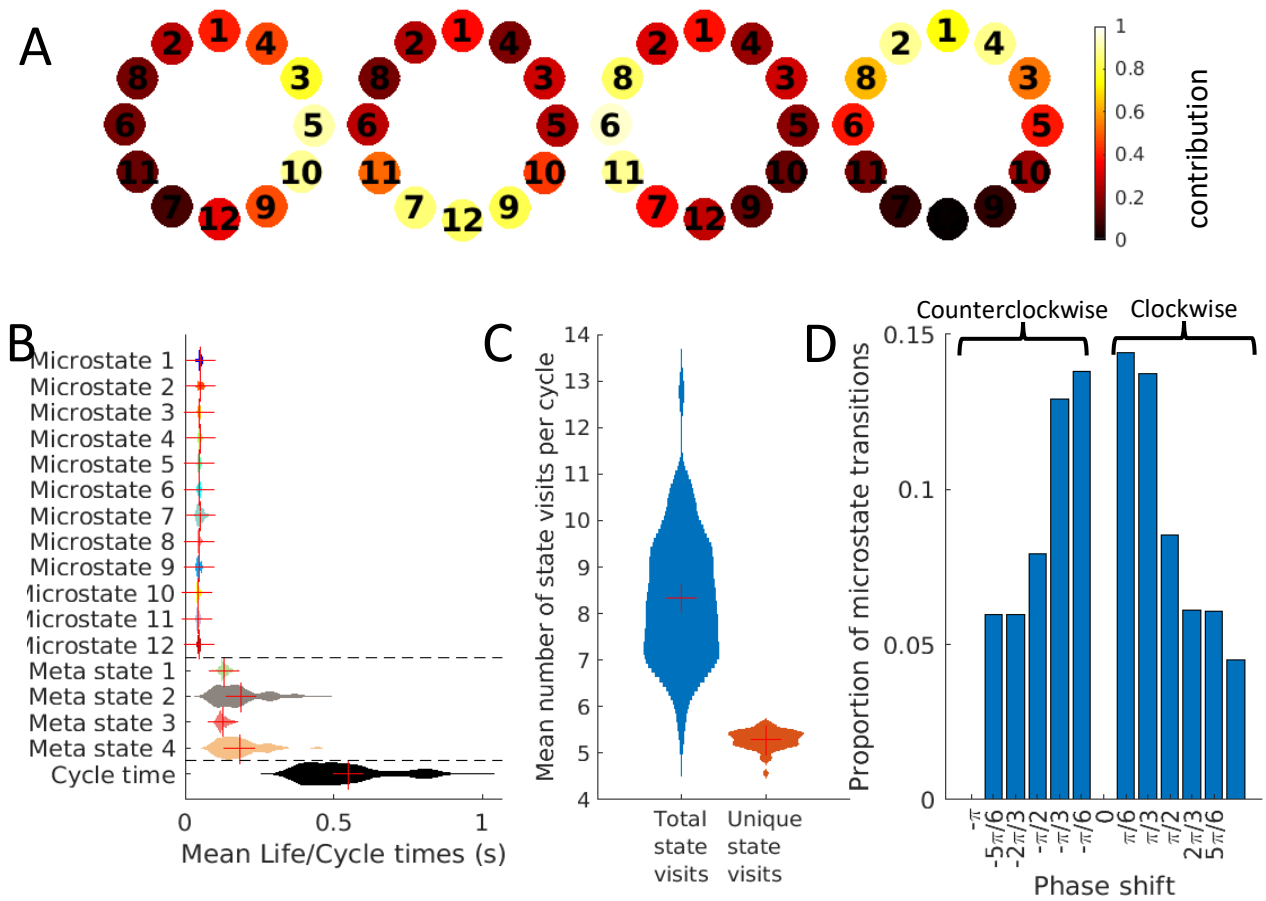

Figure 5: Characterizing individual cycle traversals. A) we fit a second level HMM model, where the four meta states (Figure 4B-C) are activated sequentially. B) The group average mean cycle duration is 8.7 times larger than the group average lifetime of a network state. C) A typical cycle traversal involves 8.7 state visits, only 5.4 of which are unique. D). Histogram of individual state transitions represented as phase-shifts on the sequential clock face; clockwise transitions are represented as positive phase shifts, whereas anticlockwise transitions are represented as negative phase shifts. This shows that the net clockwise movement is subtle but consistent, such that cyclical dynamics emerge alongside quite stochastic short-term dynamics.

We then investigated whether these temporal statistics relate to individual traits. We first took advantage of the large and equally distributed age range (18-86 years) and sex in the Cam-CAN dataset and asked whether either could be predicted by cycle rate or cycle strength (Figure 6). A General Linear Model (GLM) revealed that cycle rate reliably predicted age (beta = -4.0, t(606) = -2.53, p = 0.012), and sex (beta = 0.90, t(606) = 3.47, p = 0.0006), and that cycle strength also predicted age (beta = 0.56, t(606) = 3.12, p = 0.0018) but not sex (beta = -0.014, t(606) = -0.51, p = 0.61). A post-hoc analysis revealed that the correlation between age and cycle strength can be explained by a combination of 1) stronger pairwise asymmetries between states on average, and 2) fewer deviations from the cycle structure (i.e., fewer backwards or random transitions) (Fig S8).

Because these correlations suggest that cycle dynamics are linked to processes that unfold over the life span and are different in males and females, we wondered whether they are

genetically determined. We tested this in the HCP dataset, which contains data of mono- and dizygotic twins, and unrelated pairs of subjects using an ACE model of heritability (Chen et al., 2017; Eaves et al., 1999). The ACE aims to partition the phenotypic variance into three components: additive genetic variance (A), shared environmental factors (C), and nonshared environmental factors (E). We regressed out age and sex from the cycle metric to make sure that the relationships found with these demographics would not bias our results. Despite the relatively small cohort of twin data, we found strong evidence that cycle rate is heritable. In fact, 83% of the variance in cycle rate between twins could be explained by genetic factors ($h^2 = 0.83$, $p = 0.0039$). We did not find such an effect for cycle strength ($h^2 = 0.0$, $p = 1$), nor did we find evidence that environmental factors affected cycle metrics. Lastly, we ran canonical correlation analysis on cognitive scores in Cam-CAN to see if cyclical summary metrics are related to an individual's cognitive abilities (Smith et al., 2015; Vidaurre et al., 2017). This analysis confirmed a significant relationship between cycle metrics and cognitive scores $p = 0.0088$ (Figure 6G). Notably, where the correlation between cycle strength/rate and age had opposite signs, so did the correlation with cognitive scores after accounting for age, which could suggest a relationship between cycle dynamics and age-related cognitive decline.

In summary, the results presented here indicate that the cyclical structure Is an inherent property of human brain activity, and its dynamics are strongly rooted in our biology and might be implicated in age-related changes in cognition.

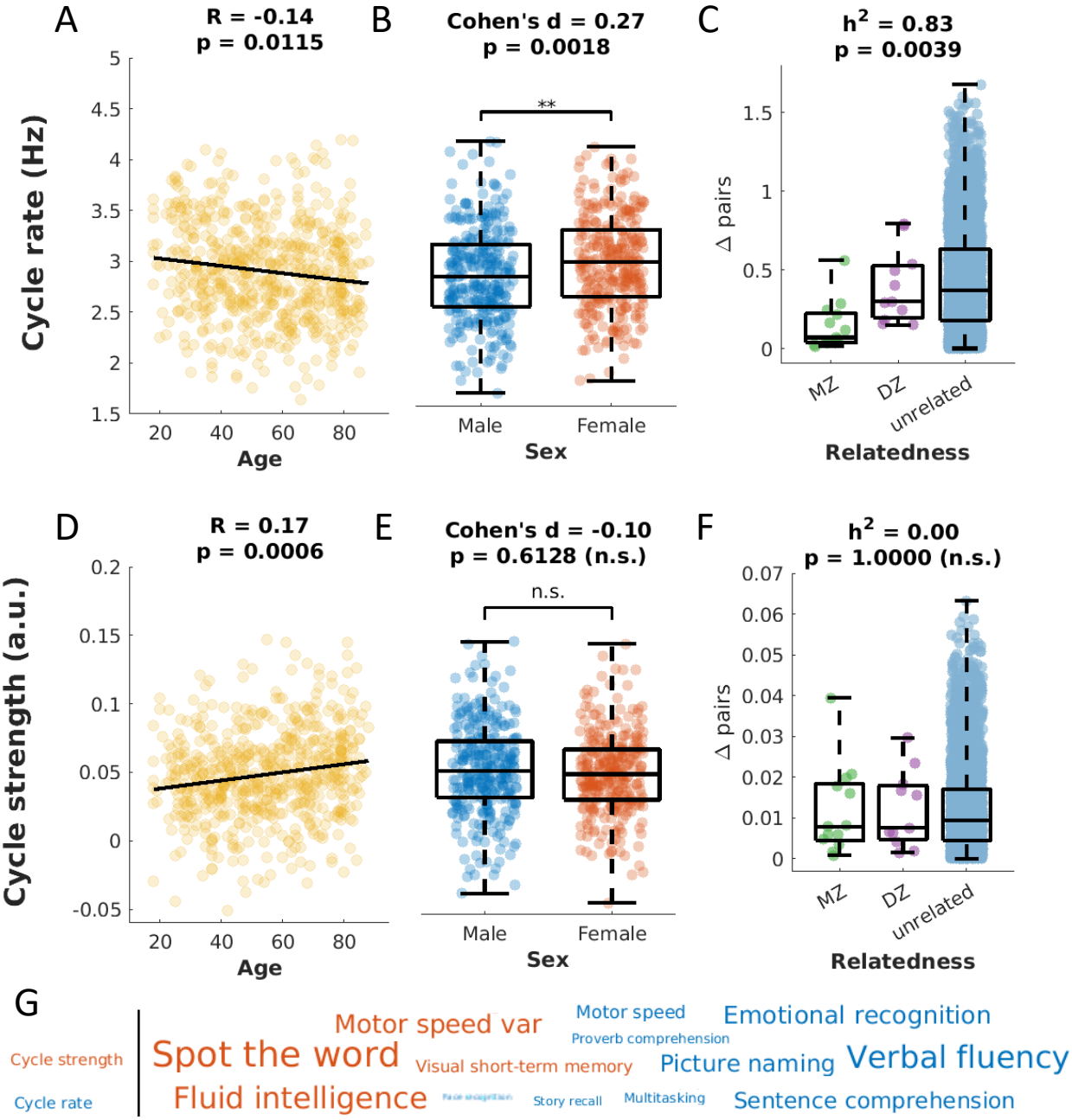

Figure 6. Cyclical activation statistics relate to individual traits and are heritable. A) Cycle rate increases with age. B) Females have a faster cycle rate than males. C) The absolute difference in cycle rate between monozygotic (MZ; "identical") twins is smaller than for Dizygotic (DZ; "non-identical") twins or unrelated subject pairs. An ACE model confirmed that cycle rate is heritable. Cycle strength is stronger in older people (D) but does not differ between males and females (E) and is not heritable (F). Circles correspond to individual subjects, boxplots display the median, 25th and 75th percentile, and whiskers indicate the minimal and maximal value. G) Cycle metrics (left) are correlated with cognition (right; p=0.0088). Red (blue) colors indicate positive (negative) correlations, word size corresponds to size of the correlation.

Preserved cycle structure in task data is cognitively relevant

Finally, given the association between cognitive traits and cycle statistics, we asked whether cyclical dynamics were relevant in cognitive task data. While the cyclical structure and the embedding of network states within it is robust across multiple datasets, it is unclear whether it persists beyond the resting brain. We therefore applied TINDA to two further datasets: a memory replay dataset (Liu et al., 2019), and a visual task dataset (Wakeman and Henson, 2015).

In the memory replay dataset, participant learned sequences structures in visual images. The representations of these have been shown to replay during a subsequent rest period (Liu et al., 2019), and recent work in our lab showed that four states in particular co-activated with memory replay; these were the DMN (state 1 in this study), parietal alpha (state 2), frontal (state 3), and visual (state 4) (Higgins et al., 2021), while most other states were less likely to be active. Interestingly, the states that have the strongest positive relationship with memory replay are clustered in the North face of the circle, while the strongest negatively correlated states are on the opposite phase (Figure 5A). This shows that cycle phase is relevant for cognition.

Memory replay has been shown to be relevant for cognition, but it does not involve any active behavior. Therefore, we also next applied TINDA to a dataset which contains an active task element. In the Faces dataset (Wakeman and Henson, 2015), 19 participants saw a series of famous, unfamiliar, or scrambled faces and had to report their asymmetry with a button press. Previous work in our lab has shown task-evoked network dynamics in this dataset (Quinn et al., 2018). Considering the current findings, we wondered whether this task structure would disrupt the cycle structure we observed in rest, and if not, whether the phase of the cycle would be relevant for task performance.

Despite the trial structure, we again confirmed the presence of an overall cyclical structure in network state activation (cycle strength higher than expected by chance; $p < 0.001$), and we also observed that the ordering of states along the cycle replicated that of the MEG UK dataset ($p = 0.027$; Figure 5B). We then correlated the state time courses time locked to button press with the reaction times for each trial. State time courses were significantly correlated ($p<0.001$), and like the replay dataset, we found opposite signs of the correlation in clusters on opposite sides of the cycle (Figure 5C). In particular, if there was a high probability that a low power state was active shortly before the button press, responses were slower, and vice versa for high power visual/attentional states.

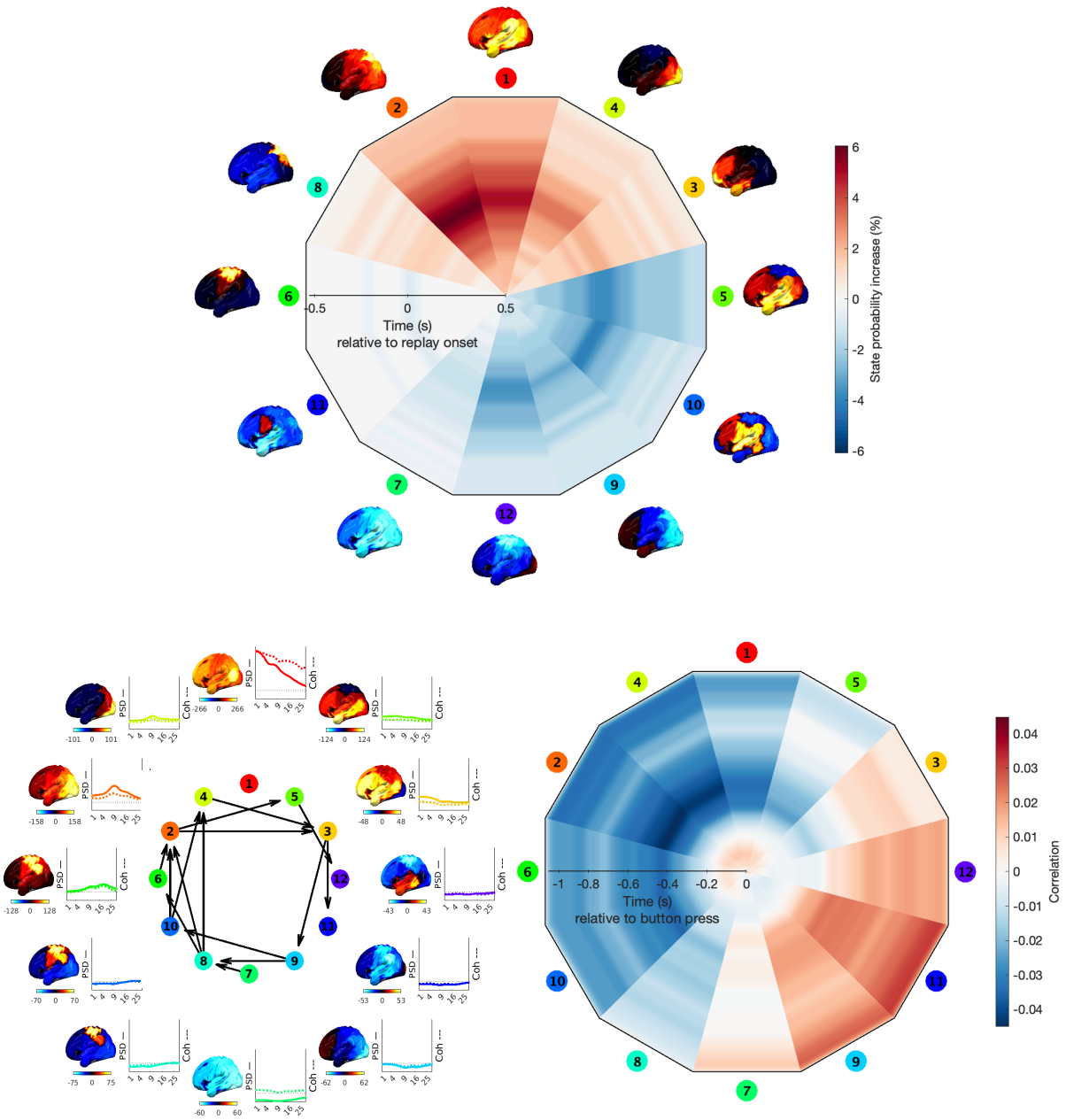

Figure 7. Cycle phase is relevant for cognition. A) The memory replay associated network states found in (Higgins et al., 2021) are clustered on one side of the cycle structure found in the MEG UK dataset (Figure 2B). Circle eccentricity shows time. B) Cycle structure comparable to those found in resting state was also found during an active task, where the correlation between reaction times and state activation probability before the button press was clustered in particular phases of the cycle.

Discussion

We have presented a new method for investigating long term structure in MEG data, based on the asymmetry in a signal's fractional occupancy (FO) during the intervals of a discrete signal (e.g., an HMM state time course). When we applied this method to multiple resting and task MEG datasets, they consistently revealed that functional brain networks have unique transition patterns that are robust across irregular time intervals, and most prominent on time scales larger than 100 ms. Together, these activation asymmetries form a cyclical activation pattern, with distinct spatio-spectral characteristics embedded within its phase that is relevant for cognition. We further found that the cyclical summary metrics are related to individual traits, are heritable, and are related to an individual's cognitive scores. Together, these findings suggest that the cyclical progression through functional brain networks during rest might be an inherent characteristic of human brain activity that is relevant for cognition.

Hierarchies in resting state networks

Within the cyclical structure, the default mode network (DMN) and dorsal attention network (DAN), which are the highest and lowest power states respectively, were consistently situated on opposite sides of the cycle. This is in line with previous MEG and fMRI studies where DAN and DMN were shown to be anticorrelated and unlikely to transition into each other directly (Baker et al., 2014; Fox et al., 2005; Margulies et al., 2016; Smith et al., 2009).

In addition, our analysis showed that the states that were embedded in between these extrema had characteristic spatio-spectral features. Specifically, the states in between DMN to DAN activation are mostly associated with higher order cognitive functioning, whereas the states in between DAN to DMN activation were related to perceptual and attentional processing. Thus, a full traversal of a cycle may begin with DMN activation, in which coherent oscillatory activity connects multimodal regions of the brain. This is followed by coherent delta/theta band activity in higher order cognitive areas, linked to top-down cognitive control and language production. This tends to be followed by widespread desynchronization of oscillatory activity, possibly coinciding with DAN activation and a reorientation of attention towards the external environment. Finally, these low-power states tend to be followed by sensorimotor beta band and then parietal alpha band activity, broadly associated with task-set maintenance (Engel and Fries, 2010) and inhibition of sensory inputs (Jensen and Mazaheri, 2010).

A dissociation of resting state networks (RSNs) into cognitive and perceptual clusters or "meta states" has previously been shown in fMRI (Bijsterbosch et al., 2017; Doucet et al., 2011; Margulies et al., 2016; Vidaurre et al., 2017). In particular, states within the perceptual/cognitive clusters were highly correlated in terms of temporal occurrence (Bijsterbosch et al., 2017; Vidaurre et al., 2017) and connectivity profile (Margulies et al., 2016), but not in states between clusters. While fMRI and MEG have different biophysical origins and temporal sensitivity, the spatial extent of RSNs is remarkably similar (Baker et al., 2014; de Pasquale et al., 2010; Quinn et al., 2018), which might be explained by the scale-free nature of human brain activity at time scales of ~250 ms to multiple seconds (Van De Ville et al., 2010). Moreover, these time scales, in addition to the observation that amplitude fluctuations in MEG can best be described by network interactions at similar time

scales (Baker et al., 2014) fits well with our finding that the cyclical structure was strongest when considering state interval times of hundreds of milliseconds to multiple seconds. Thus, the typical time scale at which the cyclical structure appears and the embedding of perceptual/cognitive RSNs in different phases of the cycle is consistent with previous fMRI and M/EEG literature.

Cycle dynamics and age

We have shown that summary metrics of the cyclical pattern are related to an individual's age and sex. In particular, cycle rate was lower in older individuals, and cycle strength was higher. This is in line with cognitive slowing and a general decline in cognitive flexibility seen in aging (Magnusson and Brim, 2014). While we did find correlation between cycle dynamics and cognitive scores, these do not unequivocally confirm these relationships.

There are several things that could shed more light on these findings. For example, one possibility is that we find differences across age groups because younger and older individuals differ in the ordering of states that make the strongest cycle. We excluded this possibility when we observed that the correlation between cycle strength and age persisted when optimizing the ordering of states either for the 100 youngest, or 100 oldest individuals (data not shown). Another analysis showed that the overall switching rate between network states decreases with age, which could explain the decrease in cycle rate.

Other age-dependent changes in brain activity are ubiquitous and include a slowing in the power spectrum (Quinn et al., 2023), and a decrease in network connectivity (Q. Chen et al., 2019; Geerligs et al., 2015; He et al., 2020; King et al., 2018; Schlesinger et al., 2017, Gohil et al. 2023), which has been related to a decrease in the segregation of functional networks. A post-hoc analysis of the current data (Fig S9) showed an overall decrease in cycle strength and increase in rate for states that decrease in connectivity with age, and the opposite for states of which connectivity increased with age. This points to a more complex interplay between the connectivity and temporal dynamics of RSNs and age than previous research suggests, which warrants future research in this area.

Heritability of cycle metrics

We showed that the variance in cycle rate amongst individuals can partly be explained by genetics. Other heritable components to large-scale brain networks have been shown in the past, including connectivity in specific functional networks (Adhikari et al., 2018; Barber et al., 2021; Fu et al., 2015; Glahn et al., 2010; Vidaurre et al., 2017), and frequency bands (Schutte et al., 2013), and static connectivity (Smit et al., 2008). In particular, Vidaurre et al. found that the degree to which an individual spent more time in either perceptual or cognitive fMRI resting states was heritable. In the subset of those same individuals for which we had MEG data available, we did not find any differences in cycle metrics between the perceptual and cognitive fMRI groups.

Relevance for cognition

We found that cyclical dynamics were present in resting state MEG data and persisted in task data. Moreover, the phase within the cycle relative to the timing of a cognitive event was shown the be relevant. This provides a more holistic view on event-locked analyses done with HMMs, as have been successfully used in the past (Higgins et al., 2021; Quinn et

al., 2018) , by showing that the states that have a meaningful relationship with the cognitive event in question are clustered in cycle space.
In future work, we intend to further investigate the temporal order of network activity relative to task, for example by expanding the TINDA method to investigate fractional occupancy between different events at different time scales, and by investigating under which conditions the cycle dynamics change (i.e., disrupt, speed up, phase reset, etc.).

Methods

All analyses were carried out in MATLAB ("MATLAB," 2020) and Python, using in-house developed software packages OHBA Software Library ("OSL MATLAB," n.d.; Quinn et al., 2022), HMM-MAR, OSL-dynamics (Gohil, 2023). The TINDA package is available for MATLAB (van Es and Higgins, 2023), and Python (Gohil, 2023).

Data

We used data from five MEG datasets: Nottingham MEG UK (N = 55), Cam-CAN (N = 612), HCP (N = 79), Replay (N=43), and Wakeman-Henson (N=19). MEG UK, Cam-CAN, HCP and replay contain MEG resting state data, Replay and Wakeman-Henson MEG task data, and all but the replay dataset include T1 weighted MRI brain scans. Datasets include demographic data and in the case of HCP, heritability data. Ethics and consent details are outlined separately for each of these datasets below.

MEG UK

The UK MEG Partnership data comprised 77 healthy participants recruited at the University of Nottingham, of which 55 were used after discarding 22 subjects because of excessive head movements or artefacts. The dataset contains structural MRI scans and MEG data from a CTF MEG system containing 275 axial gradiometers with a sampling frequency of 1200 Hz. The participant group had a mean age of 26.5 years (range 18-48). 20 of them were female, and 35 of them were male. All participants gave written informed consent and ethical approval was granted by the University of Nottingham Medical School Research Ethics Committee. The MEG data comprised roughly 5 to 6 minutes eyes-open resting state and has previously been used to characterize MEG resting state network dynamics (Higgins 2021, Hunt 2016, Vidaurre 2018).

Cam-CAN

The Cambridge Centre for Aging Neuroscience (Cam-CAN) dataset comprised data of 700 healthy participants recruited at the University of Cambridge, of which 612 were used here. The dataset contains structural MRI scans and MEG data from an Elekta Neuromag Vectorview system containing 102 magnetometers and 204 orthogonal planar gradiometers, with a sampling rate of 1 kHz. The participants were aged 18-88, with 83-95 participants per age decile (except in the 18-28 decile, which counts 45), 310 were male and 302 were female, equally distributed across the age deciles. All participants gave written informed consent and ethical approval was granted by the Cambridgeshire Research Ethics Committee. The MEG data comprised of approximately 9 minutes eyes-closed resting state.

HCP

The MEG component of the Human Connectome Project (HCP) comprised 100 healthy participants recruited at the Saint Louis University, of which 79 were used after discarding [XXX]. The dataset contains structural MRI scans and MEG data from a 4D Neuroimaging MAGNES 3600 MEG system containing 248 magnetometers sampled at 2 kHz. The participant group had a mean age of 29 (range 22-35) of which 37 females and 42 males and contained data of 13 monozygotic twin pairs and 11 dizygotic twin pairs. All participants gave written informed consent and ethical approval was granted by the local ethics committee. The MEG data comprised of three times 6 minutes of eyes-open resting state.

Replay

The Replay data (Liu et al., 2019) contained a primary dataset (dataset 1), and a replication dataset (dataset 2). For both datasets, participants were scanned on a 275 channel CTF MEG system while engaged in a localizer task, a sequence learning task, and periods of rest. Activations corresponding to images in the localizer task were found to replay during rest, in the sequence that corresponded to the learned sequences. The top 1% replay probabilities were here defined as the memory replay events, as in (Higgins et al., 2021). Replay dataset 1, was acquired from 25 participants with a mean age of 24.9 (range 19-34) of which 11 males and 14 females. Four subjects were excluded due to large motion artifacts or missing trigger information. All participants signed written consent in advance; ethical approval for the experiment was obtained from the Research Ethics Committee at University College London under ethics number 9929/002. Replay dataset 2 was acquired from 26 participants with a mean age of 25.5 (range 19-34) of which 10 males and 16 females. Four participants were later excluded due to motion artifacts or failure to complete the task. All participants signed written consent in advance; ethical approval for the experiment was obtained from the Research Ethics Committee at University College London under ethics number 9929/002. In the current study, replay dataset 1 and 2 were analyzed jointly.

Wakeman-Henson

The Wakeman-Henson faces dataset comprised MEG data acquired on an Elekta Neuromag Vectorview system of 19 participants. Of these, 8 were female, and 11 were male, and the sage range was 23-37 years. All participants gave written informed consent, and ethical approval was obtained from the Cambridge University Psychological Ethics Committee. Each participant completed six sessions of a perceptual task in which they would see a famous, familiar, or scrambled face, to which they had to respond based on the symmetry of the image. Each trial begins with a fixation cross onset between 400 and 600 ms before a target stimulus appears. The target is either the face or scrambled face stimulus and remains onscreen for between 800 and 1000 ms. Further details can be found in (Wakeman and Henson, 2015)

Preprocessing

MEG data were co-registered to the MRI structural scans, or to fiducial markers in the Replay data where MRI structural scans were not available. The MEG UK and Cam-CAN data were downsampled to 250 Hz, filtered in the 1-45 Hz range, and source-reconstructed using an LCMV beamformer to 3559 dipoles. The dipoles were then combined into 38 parcels spanning the entire cortex by taking the first principal component of all dipoles in a parcel. This parcellation was used previously to estimate large-scale static functional connectivity networks in MEG (Colcough, 2016). The HCP data were downsampled to 240 Hz, filtered in the 1-80 Hz range, and source-reconstructed using an LCMV beamformer to 5798 dipoles.

The dipoles were then combined into 78 parcels of the AAL parcellation (XXX) spanning the entire cortex by taking the first principal component of all dipoles in a parcel. Bad segments were removed manually and correction for spatial leakage was applied using symmetric multivariate leakage correction (Colcough et al, 2015). Finally, the potential inconsistency over subjects of ambiguous source polarity was removed using sign-flipping based on lagged partial correlations (Quinn et al., 2018).

Hidden Markov modelling

In order to find large scale brain networks in a data driven way, we applied a time delay embedded hidden Markov model (TDE-HMM) with 12 states and 14 embeddings, corresponding to lags of -28 to +28 ms (-29 to +29 ms for HCP). The HMM framework is a generative model that assumes there exist a finite number ($\boldsymbol{K}$) of recurring, transient, and mutually exclusive hidden states that generate the observed data. Here, each state is characterized by a spatio-spectral profile (i.e., in terms of PSD and connectivity in/across regions). Thus, every time point in the data is associated with one of the states $[\mathbf{1}, : \mathbf{2}, \dots \ \boldsymbol{K}]$, and the sequence of states is assumed to be Markovian. This means that the state active at time point $\boldsymbol{t}$ only depends on the state active at $\boldsymbol{t} - \mathbf{1}$, captured by the transition probability between all states. We used a multivariate Gaussian observation model with zero mean. Models were inferred separately for the MEG UK, Cam-CAN, and HCP datasets. For the Replay datasets, we kept the model from the MEG UK dataset fixed, and subsequently fitted it to the replay data, as in Higgins et al. (2021). Note that the state numbers in Higgins et al. (2021) were reordered in the current study based on average wideband coherence (from high to low).

Spectral analysis

We estimated the spectral information (PSD and coherence) for each state by fitting a multitaper to the original, parcellated data, condition on the active functional brain network, as in Vidaurre et al. (2016). The multitaper used a taper window length of 2 s, a frequency range of 1 to 45 Hz with a 0.5 Hz resolution (i.e., applying 7 Slepian tapers). The dimensionality of this information was reduced using spectral mode decomposition, resulting in spatial power and coherence maps for a data-driven set of frequency band modes. This decomposition is implemented by non-negative matrix factorization as detailed in Quinn et al. (2018), and Vidaurre et al. (2018). We fitted this with two modes to separate wideband activity from high frequency noise (Figure S8). We then used the wideband mode to weight the frequencies of the individual states when producing topographies.

Temporal Interval Network Density Analysis (TINDA)

We developed the TINDA method to analyze inter-state dynamics in the context of dispersive inter-state intervals. We first partition all observed interstate intervals, defining $T_{1,i}$ to be the set of timepoints that fall within the first half of interstate intervals for state i; and $T_{2,i}$ to be the set of all timepoints that fall within the second half of these interstate intervals. We then compute the $\boldsymbol{K} \times \boldsymbol{K}$ fractional occupancy asymmetry matrix ($\boldsymbol{A}$), defined as the matrix whose (i,j)th entry is:

$$A_{i,j} = P\left(z_t = j \middle| t \in T_{1,i}\right) - P(z_t = j | t \in \ T_{2,i})$$

Where $P(z_t = j | t \in T_{1,i})$ is the proportion of timepoints in the set that were assigned to state j. These Fractional Occupancy Asymmetry matrices are computed for each subject.

Cycle detection and Cycle Strength

TINDA establishes whether there is a general flow of states into and out of a particular state. We investigated whether this pattern is embedded in a larger, hierarchical structure, specifically a cycle. We interpret the fractional occupancy asymmetry matrix, A, as a weighted, directed graph of $\boldsymbol{K}$ nodes (i.e., number of states) and $\boldsymbol{K^2} - \boldsymbol{K}$ edges (i.e., from every node to every other node). The fractional occupancy asymmetry thus defines the weight and direction of each edge.

To investigate how these edges relate to specifically cyclical dynamics, we define a metric of cycle strength for each configuration of the $\boldsymbol{K}$ nodes around the unit circle. Each node is associated with a phase θ, positioned on the unit circle in $\frac{2\pi}{K}$ intervals, spanning $[0, 2\pi]$. We can then represent each directed transition, from state n to state m, by a vector in the complex plane defined by the phase difference between the relative position of nodes m and n:

$$d_{m,n} = e^{i(\theta^m - \theta^n)} \qquad [5]$$

The magnitude of the imaginary component of this vector represents a geometric projection of each state transition onto the plane tangential to the unit circle at node n. Trivially, the cumulative sum of these vectors for all $\boldsymbol{n}$ and $\boldsymbol{m}$ is zero. However, if these vectors are weighted by the strength (and direction) of the corresponding FO asymmetry, then the sum of their imaginary components represents the cumulative strength (i.e., of the asymmetry) and the polarity represents the net direction (i.e., clockwise (+) vs. counterclockwise (-)) of transitions tangential to the unit circle. Hence, we define the cycle strength, S, is defined as:

$$S = -\beta \times \sum_m \sum_{n \neq m} A^{m,n} \times \sin(\theta^m - \theta^n) \qquad [6]$$

Where β is a normalization factor based on the theoretical maximum cycle strength for $\boldsymbol{K}$ states, such that $\boldsymbol{S}$ is constrained to be [-1, 1]. The theoretical maximum cycle strength is computed for K states by assuming a perfect asymmetry of +1 for all possible clockwise connections, and -1 for all possible negative connections.
We permuted the position of each state on the unit circle (i.e., the node identity) in order to maximize $\boldsymbol{S}$. This reveals the sequence of states for which the overall directionality is maximal in the clockwise direction. Note that we could have chosen to maximize negative $\boldsymbol{S}$ instead. This would have only resulted in all circle plots going in a counterclockwise direction; it would not have changed any of our results.

Circle plots

The circle plots all show the states in the sequence which maximizes the cycle strength (in clockwise direction). The edges $\boldsymbol{E}$ that are shown are those where the fractional occupancy asymmetry is statistically significant (see Statistics), where the direction of the arrow depends on the sign of the corresponding edge asymmetry, where $\boldsymbol{\alpha}$ is the (corrected) statistical threshold (see Statistics):

$$E^{j,k} = \begin{cases} 0, & p_{j,k} \geq \alpha \\ -1, & p_{j,k} < \alpha \ \wedge \ A^{j,k} < 0 \\ +1, & p_{j,k} < \alpha \ \wedge \ A^{j,k} > 0 \end{cases} \qquad [7]$$

Cycle rate

To quantify cycle rate we applied a post-hoc analysis to the state time course parameters already learned. Specifically, we derived a feature from the state time courses defined as the number of state visits in a sliding window equal to the average state lifetime (64-68 ms, depending on the dataset). We then fit a second level HMM to this feature time course, where this HMM used a Poisson observation model and sequential Markov dynamics (Higgins et al., 2022). We selected a model with $\boldsymbol{K} = \mathbf{4}$ states, where we initialized the state probabilities as the distance (i.e., in circle space) to the centroid of each of the four modes in figure 4B-C. We also enforced a sequence of state 1 > state 2 > state 3 > state 4 > state 1, etc. such that a single cycle was defined as sequentially activation each of the four modes in Figure 4B-C. Using this initialized model, we inferred the state time courses from the data without training the model to convergence. This was done to not deviate from our definition of a "cycle", and to subsequently quantify cycle duration as the time it takes to cycle through a full 1 > 2 > 3 > 4 sequence of the second level HMM. For correlations with individual traits, the inverse (i.e., cycle rate) was used, as this was more normally distributed.

Statistics

FO asymmetry

The FO asymmetry was tested on the group level with a two-tailed dependent samples T-test for each of the connections $\boldsymbol{m}, \boldsymbol{n}$, where the alpha threshold of 0.05 was Bonferroni corrected for 132 tests (i.e., $\boldsymbol{K}^{\mathbf{2}} - \boldsymbol{K}$), resulting in a corrected alpha threshold of 0.00038. For the Replay datasets, TINDA was run on the intervals between replay events for all state activations, and vice versa. The alpha threshold for testing the FO asymmetry was corrected for 24 tests (i.e., 2*$\boldsymbol{K}$).

Cycle strength

We report the results for the sequence of states that results in the strongest, clockwise cycles. A claim of nonzero cycle strength could be a trivial consequence of this optimization. For this reason, we compared the observed cycle strength with that from permutations, where for each permutation we permuted each subjects' state labels and recomputed the FO asymmetry and optimized state ordering. Due to the computational cost of optimizing the state ordering, this was done 100 times. The observed cycle strength was compared with the permuted versions at alpha=0.05.

Circle plots

Circle plots show the edges where the FO asymmetry is strongest (and significant). For the MEG UK dataset, all significant edges are shown. For Cam-CAN, the edges with absolute t-values larger than 11 are shown (corresponding to a p-value smaller than $3.8*10^{-20}$), and for the HCP dataset the edges with absolute t-values larger than 4.3 (corresponding to p-values smaller than $3.8*10^{-5}$).

Correlation with individual traits

For the correlation of cycle rate and cycle strength with individual traits, outliers more than three standard deviations from the mean value were removed prior to the general linear model (GLM). We fitted a mean term, and the cycle rate and cycle strength to age and sex separately, using a Gaussian and binomial distribution, respectively. Beta terms for each were significant if the corresponding p-value was lower than the alpha threshold of 0.0125 (i.e., 0.05 corrected for 4 tests).

Heritability

In order to test whether variance in cycle metric could be explained by genetic factors, we used an ACE model, as implemented in the Accelerated Permutation Inference for the ACE Model (APACE) framework (X. Chen et al., 2019). Prior to running the model, we regressed out age, and sex, from the cycle metrics. APACE was run on all subjects' cycle metrics for the three resting state sessions, separately for cycle rate, and cycle strength, using 10000 permutations. Alpha thresholds of 0.05 were Bonferroni corrected for two tests.

Correlation with cognitive scores

A canonical correlation analysis (CCA) was executed on Cam-CAN dataset, between the cyclical symmary metrics (cycle rate and strength) on the one hand, and thirteen cognitive scores on the other hand. For all metrics, we first regressed out age, and sex, and then z-transformed the data. The CCA resulted in two CCA components, which were tested for significance by comparing against a permutation distribution of 10000 permutations, where for each permutation, the cognitive scores were shuffled over subjects.

Correlation between state probability and reaction times

We time locked the state probability time courses to the button presses in the Wakeman-Henson data and correlated at each time point in the [-1 0] second window, the probability with the reaction time on that trial. This was done separately for each session and state, after which we averaged the correlations over sessions for each subject. We repeated this analysis 100 times with permuted reaction times, and averaged over these permutations to create a null. The comparison against the null was done using non-parametric permutation tests with 10000 permutations, where neighboring states in cycle space and neighboring time points were clustered. For visualizing, image plots were smoothed using a 2D Gaussian filter.

Acknowledgements

The authors would like to thank Thomas Nichols and Xu Chen for their help in using the APACE model. This research was funded by the Wellcome Trust (106183/Z/14/Z, 215573/Z/19/Z), the New Therapeutics in Alzheimer's Diseases (NTAD) study supported by UK MRC and the Dementia Platform UK (RG94383/RG89702) and the

EU-project euSNN (MSCA-ITN H2020-860563), and supported by the NIHR Oxford Health Biomedical Research Centre. DV is supported by a Novo Nordisk Emerging Investigator Award (NNF19OC-0054895) and by the European Research Council (ERC-StG-2019-850404). The Wellcome Centre for Integrative Neuroimaging is supported by core funding from the Wellcome Trust (203139/Z/16/Z and 203139/A/16/Z). For the purpose of open access, the author has applied a CC BY public copyright licence to any Author Accepted Manuscript version arising from this submission.

References

Adhikari, B.M., Jahanshad, N., Shukla, D., Glahn, D.C., Blangero, J., Fox, P.T., Reynolds, R.C., Cox, R.W., Fieremans, E., Veraart, J., Novikov, D.S., Nichols, T.E., Hong, L.E., Thompson, P.M., Kochunov, P., 2018. Comparison of heritability estimates on resting state fMRI connectivity phenotypes using the ENIGMA analysis pipeline. Hum Brain Mapp 39, 4893–4902. https://doi.org/10.1002/hbm.24331

Andrews-Hanna, J.R., 2012. The Brain's Default Network and Its Adaptive Role in Internal Mentation. Neuroscientist 18, 251–270. https://doi.org/10.1177/1073858411403316

Baker, A.P., Brookes, M.J., Rezek, I.A., Smith, S.M., Behrens, T., Smith, P.J.P., Woolrich, M., 2014. Fast transient networks in spontaneous human brain activity. eLife 2014, 1–18. https://doi.org/10.7554/eLife.01867

Barber, A.D., Hegarty, C.E., Lindquist, M., Karlsgodt, K.H., 2021. Heritability of Functional Connectivity in Resting State: Assessment of the Dynamic Mean, Dynamic Variance, and Static Connectivity across Networks. Cerebral Cortex 31, 2834–2844. https://doi.org/10.1093/cercor/bhaa391

Bijsterbosch, J., Harrison, S., Duff, E., Alfaro-Almagro, F., Woolrich, M., Smith, S., 2017. Investigations into within- and between-subject resting-state amplitude variations. NeuroImage 159, 57–69. https://doi.org/10.1016/j.neuroimage.2017.07.014

Braun, U., Schäfer, A., Walter, H., Erk, S., Romanczuk-Seiferth, N., Haddad, L., Schweiger, J.I., Grimm, O., Heinz, A., Tost, H., Meyer-Lindenberg, A., Bassett, D.S., 2015. Dynamic reconfiguration of frontal brain networks during executive cognition in humans. Proc. Natl. Acad. Sci. U.S.A. 112, 11678–11683. https://doi.org/10.1073/pnas.1422487112

Buckner, R.L., Andrews-Hanna, J.R., Schacter, D.L., 2008. *The Brain's Default Network*: *Anatomy, Function, and Relevance to Disease*. Annals of the New York Academy of Sciences 1124, 1–38. https://doi.org/10.1196/annals.1440.011

Cam-CAN, Shafto, M.A., Tyler, L.K., Dixon, M., Taylor, J.R., Rowe, J.B., Cusack, R., Calder, A.J., Marslen-Wilson, W.D., Duncan, J., Dalgleish, T., Henson, R.N., Brayne, C., Matthews, F.E., 2014. The Cambridge Centre for Ageing and Neuroscience (Cam-CAN) study protocol: a cross-sectional, lifespan, multidisciplinary examination of healthy cognitive ageing. BMC Neurol 14, 204. https://doi.org/10.1186/s12883-014-0204-1

Chen, Q., Xia, Y., Zhuang, K., Wu, X., Liu, G., Qiu, J., 2019. Decreased inter-hemispheric interactions but increased intra-hemispheric integration during typical aging. Aging 11, 10100–10115. https://doi.org/10.18632/aging.102421

Chen, X., Formisano, E., Blokland, G.A.M., Strike, L.T., McMahon, K.L., Zubicaray, G.I., Thompson, P.M., Wright, M.J., Winkler, A.M., Ge, T., Nichols, T.E., 2019. Accelerated estimation and permutation inference for ACE modeling. Hum Brain Mapp 40, 3488–3507. https://doi.org/10.1002/hbm.24611

Chen, X., Viding, E., Nichols, T., 2017. Faster Accelerated Permutation Inference for the ACE Model (APACE) with Parallelization. figshare. https://doi.org/10.6084/M9.FIGSHARE.5473174.V1

Colom, R., Karama, S., Jung, R.E., Haier, R.J., 2010. Human intelligence and brain networks. Dialogues in Clinical Neuroscience 12, 489–501. https://doi.org/10.31887/DCNS.2010.12.4/rcolom

de Pasquale, F., Della Penna, S., Snyder, A.Z., Lewis, C., Mantini, D., Marzetti, L., Belardinelli, P., Ciancetta, L., Pizzella, V., Romani, G.L., Corbetta, M., 2010. Temporal dynamics of spontaneous MEG activity in brain networks. Proc. Natl. Acad. Sci. U.S.A. 107, 6040–6045. https://doi.org/10.1073/pnas.0913863107

Doucet, G., Naveau, M., Petit, L., Delcroix, N., Zago, L., Crivello, F., Jobard, G., Tzourio-Mazoyer, N., Mazoyer, B., Mellet, E., Joliot, M., 2011. Brain activity at rest: a multiscale hierarchical functional organization. Journal of Neurophysiology 105, 2753–2763. https://doi.org/10.1152/jn.00895.2010

Eaves, L., Heath, A., Martin, N., Maes, H., Neale, M., Kendler, K., Kirk, K., Corey, L., 1999. Comparing the biological and cultural inheritance of personality and social attitudes in the Virginia 30 000 study of twins and their relatives. Twin res. 2, 62–80. https://doi.org/10.1375/twin.2.2.62

Engel, A.K., Fries, P., 2010. Beta-band oscillations—signalling the status quo? Current Opinion in Neurobiology 20, 156–165. https://doi.org/10.1016/j.conb.2010.02.015

Fox, M.D., Snyder, A.Z., Vincent, J.L., Corbetta, M., Van Essen, D.C., Raichle, M.E., 2005. The human brain is intrinsically organized into dynamic, anticorrelated functional networks. Proc. Natl. Acad. Sci. U.S.A. 102, 9673–9678. https://doi.org/10.1073/pnas.0504136102

Fu, Y., Ma, Z., Hamilton, C., Liang, Z., Hou, X., Ma, X., Hu, X., He, Q., Deng, W., Wang, Y., Zhao, L., Meng, H., Li, T., Zhang, N., 2015. Genetic influences on resting-state functional networks: *A twin study*: Genetic Influences on Resting-State Functional Networks. Hum. Brain Mapp. 36, 3959–3972. https://doi.org/10.1002/hbm.22890

Geerligs, L., Renken, R.J., Saliasi, E., Maurits, N.M., Lorist, M.M., 2015. A Brain-Wide Study of Age-Related Changes in Functional Connectivity. Cerebral Cortex 25, 1987–1999. https://doi.org/10.1093/cercor/bhu012

Glahn, D.C., Winkler, A.M., Kochunov, P., Almasy, L., Duggirala, R., Carless, M.A., Curran, J.C., Olvera, R.L., Laird, A.R., Smith, S.M., Beckmann, C.F., Fox, P.T., Blangero, J., 2010. Genetic control over the resting brain. Proc. Natl. Acad. Sci. U.S.A. 107, 1223–1228. https://doi.org/10.1073/pnas.0909969107

Gohil, et al., 2023. OSL-dynamics.

He, L., Wang, X., Zhuang, K., Qiu, J., 2020. Decreased Dynamic Segregation but Increased Dynamic Integration of the Resting-state Functional Networks During Normal Aging. Neuroscience 437, 54–63. https://doi.org/10.1016/j.neuroscience.2020.04.030

Higgins, C., Liu, Y., Vidaurre, D., Kurth-Nelson, Z., Dolan, R., Behrens, T., Woolrich, M., 2021. Replay bursts in humans coincide with activation of the default mode and parietal alpha networks. Neuron 109, 882-893.e7. https://doi.org/10.1016/j.neuron.2020.12.007

Higgins, C., Vidaurre, D., Kolling, N., Liu, Y., Behrens, T., Woolrich, M., 2022. Spatiotemporally resolved multivariate pattern analysis for M/ EEG. Human Brain Mapping hbm.25835. https://doi.org/10.1002/hbm.25835

HMM-MAR, n.d.

Jensen, O., Mazaheri, A., 2010. Shaping Functional Architecture by Oscillatory Alpha Activity: Gating by Inhibition. Frontiers in Human Neuroscience 4. https://doi.org/10.3389/fnhum.2010.00186

Jouvet, M., 1967. Neurophysiology of the states of sleep. Physiological Reviews 47, 117–177. https://doi.org/10.1152/physrev.1967.47.2.117

King, B.R., Van Ruitenbeek, P., Leunissen, I., Cuypers, K., Heise, K.-F., Santos Monteiro, T., Hermans, L., Levin, O., Albouy, G., Mantini, D., Swinnen, S.P., 2018. Age-Related Declines in Motor Performance are Associated With Decreased Segregation of Large-Scale Resting State Brain Networks. Cerebral Cortex 28, 4390–4402. https://doi.org/10.1093/cercor/bhx297

Larson-Prior, L.J., Oostenveld, R., Della Penna, S., Michalareas, G., Prior, F., Babajani-Feremi, A., Schoffelen, J.-M., Marzetti, L., de Pasquale, F., Di Pompeo, F., Stout, J., Woolrich, M., Luo, Q., Bucholz, R., Fries, P., Pizzella, V., Romani, G.L., Corbetta, M., Snyder, A.Z., 2013. Adding dynamics to the Human Connectome Project with MEG. NeuroImage 80, 190–201. https://doi.org/10.1016/j.neuroimage.2013.05.056

Liu, Y., Dolan, R.J., Kurth-Nelson, Z., Behrens, T.E.J., 2019. Human Replay Spontaneously Reorganizes Experience. Cell 178, 640-652.e14. https://doi.org/10.1016/j.cell.2019.06.012

Magnusson, K.R., Brim, B.L., 2014. The Aging Brain, in: Reference Module in Biomedical Sciences. Elsevier, p. B9780128012383000000. https://doi.org/10.1016/B978-0-12-801238-3.00158-6

Mantini, D., Perrucci, M.G., Del Gratta, C., Romani, G.L., Corbetta, M., 2007. Electrophysiological signatures of resting state networks in the human brain. Proc. Natl. Acad. Sci. U.S.A. 104, 13170–13175. https://doi.org/10.1073/pnas.0700668104

Margulies, D.S., Ghosh, S.S., Goulas, A., Falkiewicz, M., Huntenburg, J.M., Langs, G., Bezgin, G., Eickhoff, S.B., Castellanos, F.X., Petrides, M., Jefferies, E., Smallwood, J., 2016. Situating the default-mode network along a principal gradient of macroscale cortical organization. Proceedings of the National Academy of Sciences 113, 12574–12579. https://doi.org/10.1073/pnas.1608282113

MATLAB, 2020.

Menon, V., 2023. 20 years of the default mode network: A review and synthesis. Neuron S0896627323003082. https://doi.org/10.1016/j.neuron.2023.04.023

Mitra, A., Raichle, M.E., 2016. How networks communicate: propagation patterns in spontaneous brain activity. Phil. Trans. R. Soc. B 371, 20150546. https://doi.org/10.1098/rstb.2015.0546

OSL MATLAB, n.d.

Quinn, A.J., van Es, M.W.J., Gohil, C., Woolrich, M.W., 2022. OHBA Software Library in Python (OSL). https://doi.org/10.5281/ZENODO.6875060

Quinn, A.J., Vidaurre, D., Abeysuriya, R., Becker, R., Nobre, A.C., Woolrich, M.W., 2018. Task-Evoked Dynamic Network Analysis Through Hidden Markov Modeling. Front. Neurosci. 12, 603. https://doi.org/10.3389/fnins.2018.00603

Schlesinger, K.J., Turner, B.O., Lopez, B.A., Miller, M.B., Carlson, J.M., 2017. Age-dependent changes in task-based modular organization of the human brain. NeuroImage 146, 741–762. https://doi.org/10.1016/j.neuroimage.2016.09.001

Schutte, N.M., Hansell, N.K., De Geus, E.J.C., Martin, N.G., Wright, M.J., Smit, D.J.A., 2013. Heritability of Resting State EEG Functional Connectivity Patterns. Twin Res Hum Genet 16, 962–969. https://doi.org/10.1017/thg.2013.55

Sepulcre, J., Sabuncu, M.R., Yeo, T.B., Liu, H., Johnson, K.A., 2012. Stepwise Connectivity of the Modal Cortex Reveals the Multimodal Organization of the Human Brain. Journal of Neuroscience 32, 10649–10661. https://doi.org/10.1523/JNEUROSCI.0759-12.2012

Sitnikova, T., Hughes, J.W., Howard, C.M., Stephens, K.A., Woolrich, M.W., Salat, D.H., 2020. Spontaneous activity changes in large-scale cortical networks in older adults couple to distinct hemodynamic morphology (preprint). Neuroscience. https://doi.org/10.1101/2020.05.05.079749

Smit, D.J.A., Stam, C.J., Posthuma, D., Boomsma, D.I., De Geus, E.J.C., 2008. Heritability of "small-world" networks in the brain: A graph theoretical analysis of resting-state EEG functional connectivity. Hum. Brain Mapp. 29, 1368–1378. https://doi.org/10.1002/hbm.20468

Smith, S.M., Fox, P.T., Miller, K.L., Glahn, D.C., Fox, P.M., Mackay, C.E., Filippini, N., Watkins, K.E., Toro, R., Laird, A.R., Beckmann, C.F., 2009. Correspondence of the brain's functional architecture during activation and rest. Proc. Natl. Acad. Sci. U.S.A. 106, 13040–13045. https://doi.org/10.1073/pnas.0905267106

Smith, S.M., Nichols, T.E., Vidaurre, D., Winkler, A.M., Behrens, T.E.J., Glasser, M.F., Ugurbil, K., Barch, D.M., Van Essen, D.C., Miller, K.L., 2015. A positive-negative mode of population covariation links brain connectivity, demographics and behavior. Nat Neurosci 18, 1565–1567. https://doi.org/10.1038/nn.4125

Spreng, R.N., Grady, C.L., 2010. Patterns of Brain Activity Supporting Autobiographical Memory, Prospection, and Theory of Mind, and Their Relationship to the Default Mode Network. Journal of Cognitive Neuroscience 22, 1112–1123. https://doi.org/10.1162/jocn.2009.21282

Spreng, R.N., Mar, R.A., Kim, A.S.N., 2009. The Common Neural Basis of Autobiographical Memory, Prospection, Navigation, Theory of Mind, and the Default Mode: A Quantitative Meta-analysis. Journal of Cognitive Neuroscience 21, 489–510. https://doi.org/10.1162/jocn.2008.21029

Taylor, J.R., Williams, N., Cusack, R., Auer, T., Shafto, M.A., Dixon, M., Tyler, L.K., Cam-CAN, Henson, R.N., 2017. The Cambridge Centre for Ageing and Neuroscience (Cam-CAN) data repository: Structural and functional MRI, MEG, and cognitive data from a cross-sectional adult lifespan sample. NeuroImage 144, 262–269. https://doi.org/10.1016/j.neuroimage.2015.09.018

UK MEG Partnership, 2016. MEG UK Database [WWW Document].

Van De Ville, D., Britz, J., Michel, C.M., 2010. EEG microstate sequences in healthy humans at rest reveal scale-free dynamics. Proc. Natl. Acad. Sci. U.S.A. 107, 18179–18184. https://doi.org/10.1073/pnas.1007841107

van Es, M., Higgins, C., 2023. TINDA.

Vidaurre, D., Abeysuriya, R., Becker, R., Quinn, A.J., Alfaro-Almagro, F., Smith, S.M., Woolrich, M.W., 2018a. Discovering dynamic brain networks from big data in rest and task. NeuroImage 180, 646–656. https://doi.org/10.1016/j.neuroimage.2017.06.077

Vidaurre, D., Hunt, L.T., Quinn, A.J., Hunt, B.A.E., Brookes, M.J., Nobre, A.C., Woolrich, M.W., 2018b. Spontaneous cortical activity transiently organises into frequency specific phase-coupling networks. Nature Communications 9. https://doi.org/10.1038/s41467-018-05316-z

Vidaurre, D., Smith, S.M., Woolrich, M.W., 2017. Brain network dynamics are hierarchically organized in time. Proc. Natl. Acad. Sci. U.S.A. 114, 12827–12832. https://doi.org/10.1073/pnas.1705120114

Wakeman, D.G., Henson, R.N., 2015. A multi-subject, multi-modal human neuroimaging dataset. Sci Data 2, 150001. https://doi.org/10.1038/sdata.2015.1